Combined Bethe-Saltpeter equations and time-dependent density-functional theory approach for x-ray absorption calculations

A. L. Ankudinov, Y. Takimoto, and J. J. Rehr
Department of Physics, University of Washington, Seattle, Washington 98195-1560, USA
(Received 23 December 2004; published 14 April 2005)

Many-body effects such as local fields and the core-hole interaction can be significant in x-ray absorption spectra even several hundred eV above an absorption edge. The treatment of these effects requires theories beyond the independent-particle approximation, e.g., the Bethe-Saltpeter equation (BSE) or the time-dependent density-functional theory (TDDFT). However the BSE is usually limited to low energies, while the TDDFT often ignores the nonlocality of the core-hole interaction. Here we present a combined approach for the calculations of the x-ray spectra that include both of these effects, together with inelastic losses and self-energy shifts over a wide energy range. The approach is illustrated for a few materials, including metals and oxides.

DOI: 10.1103/PhysRevB.71.165110 PACS number(s): 78.70.Dm, 78.20.Ls

I. INTRODUCTION

The many-body effects beyond the independent-particle approximation, in particular the core-hole photoelectron interaction and local-field effects due to the screening of the x-ray field, lead to systematic differences between the one-electron calculations of x-ray absorption spectra (XAS) and the experiment. However, the development of an efficient, yet quantitative approach for general calculations that includes these effects remains a challenge. These two-particle interactions can be treated using the Bethe-Saltpeter equation (BSE),[1–4] but this approach is computationally demanding. A more efficient method is based on the time-dependent density-functional theory (TDDFT).[5–7] This approach typically employs a local exchange-correlation functional, but nonlocality is sometimes crucial.[8] The core-hole interaction can also be treated approximately in independent-particle calculations based on the *final-state rule* (FSR), where the final states are calculated in the presence of a fully screened core hole, and other many-body effects are lumped into the photoelectron self-energy.[9] For deep-core excitations the treatment of the core hole using the FSR can yield results comparable to those from the BSE.[10] The more *ad hoc Z* $+1$ approximation[11] and transition-state[12] approaches have also been used in practice.

However, none of these approaches is fully satisfactory, as illustrated in Fig. 1 for the *M*-edge XAS of tungsten. For this material the independent particle approximation (dashes) overestimates the magnitude of the XAS and the material decays more rapidly with energy than it does in the experiment (thick solid). Adding a screened core hole within the FSR does not significantly change the results for this system, which, as shown below, is dominated by local-field effects. Eliminating such discrepancies can be of practical importance, since the amplitude of the edge jump is used, e.g., to measure the thickness of the interconnects in integrated circuits.[13] Clearly both the BSE (dots) and the TDDFT (solid) roughly account for the discrepancy close to the edge. However, numerical basis-set limitations generally restrict the BSE to relatively low energies, typically below about 200 eV of threshold. Also, the lack of sufficiently accurate exchange-correlation functionals or the neglect of their nonlocality can limit the applicability of TDDFT close to the absorption edges. Thus a number of attempts have been made to improve on the TDDFT.[4] This paper is another attempt, which succeeds in combining the TDDFT and BSE methods.

Formally the XAS cross section can be expressed in terms of the fully interacting response function as,[5]

$$\sigma(\omega) = -4\pi\frac{\omega}{c}\,\mathrm{Im}\int d\mathbf{r}d\mathbf{r}'d^{\dagger}(\mathbf{r})\chi(\mathbf{r},\mathbf{r}',\omega)d(\mathbf{r}), \qquad (1)$$

where $d(\mathbf{r})=\hat{\epsilon}\cdot\mathbf{r}$ is the dipole operator coupling to the external x-ray field, and the two-point response function is obtained by contracting the four-point response $\chi(\mathbf{r},\mathbf{r}',\omega)$

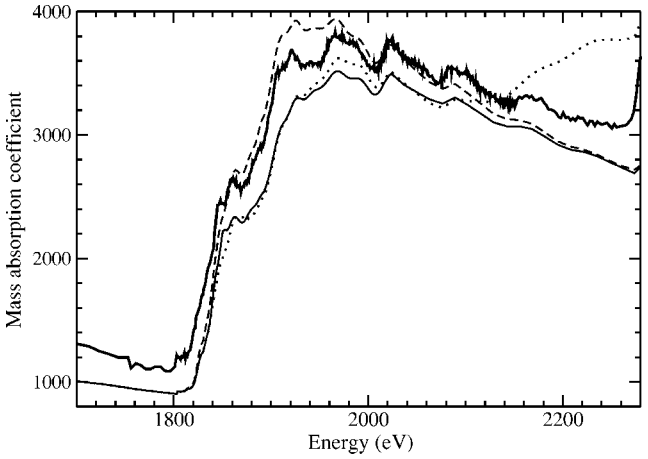

FIG. 1. Absolute measurements and calculations of the mass-absorption coefficient μ in cm^2/g near the M_5 edge of tungsten: experiment (Ref. 13) (thick solid) vs calculations based on the independent-particle approximation (dashes), on the TDDFT approach with only local-field effects (solid), and on our projection approach to the BSE (Ref. 14) (dots). The experimental uncertainty is approximately $100+0.03\ \mu\,\mathrm{cm}^2/\mathrm{g}$ (Ref. 13), which is comparable to the discrepancy between the TDDFT approach and the experiment.

$={}^4\chi(\mathbf{r},\mathbf{r}',\mathbf{r}',\mathbf{r},\omega)$. Below we will omit the superscript 4, unless it is needed for clarity. The core-hole and local-field interactions are both incorporated in the kernel K of the integral equation for the response function,

$$\chi(\omega) = \chi^0(\omega) + \chi^0(\omega)K\chi(\omega), \tag{2}$$

where here and elsewhere the matrix indices are also suppressed, unless they are needed for clarity. In Eq. (2) $\chi^0(\omega)$ is the independent particle-response function and

$$K = K^X + K^D, \tag{3}$$

is the kernel, where K^D and K^X denote the direct (i.e., particle-hole interaction) and exchange terms, respectively. These terms are of opposite signs, and hence they tend to cancel. Their relative importance reflects the different components of the response function χ, and hence one or the other can dominate, depending on the system. As discussed below, K^X typically reflects the p-wave response to the dipole coupling, while K^D reflects the s-wave character of the core hole.

Within the BSE the direct term K^D is usually taken to be the adiabatically screened Coulomb interaction,[4]

$$K^D \approx W(\mathbf{r},\mathbf{r}') = \epsilon^{-1}v(\mathbf{r},\mathbf{r}'), \tag{4}$$

where ϵ^{-1} is the static-dielectric function, as calculated within the random-phase approximation (RPA) and $v(\mathbf{r},\mathbf{r}') = 1/|\mathbf{r}-\mathbf{r}'|$ is the bare Coulomb interaction. However, the difficulty of calculating both $W(\mathbf{r},\mathbf{r}')$ and the four-point BSE response function poses severe numerical complications, often requiring large particle-hole-basis sets. Consequently the calculations become progressively more time-consuming and eventually impractical as the photoelectron energy is increased. For example, the BSE calculations based on our local-projection-operator method[14] (Fig. 1, dots) already require the inversion of order 100×100 matrices at each energy point with a double-basis set $\psi_i^*\psi_j$, including four final-state f-orbitals. As a result, this limited-basis set loses accuracy and becomes inadequate about 200 eV above the edge.

The replacement of K^D by a local-density approximation in the TDDFT approach of Zangwill and Soven[5] (ZS) greatly simplifies the calculations. In their approach the expansion in double-basis sets is circumvented, and the calculations of XAS are equivalently carried out using a Fermi[1], "golden rule" expression in which the coupling to the x-ray field is replaced by a screened local field $\tilde{d}$. Unfortunately local kernels have been found to be unsatisfactory for many systems, particularly for molecules and insulators, as stressed by several authors.[8] This drawback has provided an incentive for this and other developments.[4,10]

The plan of this article is as follows. Section II outlines our combined approach, Sec. III describes the treatment of local-field effects, Sec. IV describes the BSE and nonlocal core-hole interaction, and Sec. V relates our treatment of the statically screened core-hole interaction. Finally Sec. VI contains our results and Sec. VII contains a summary and conclusions.

II. COMBINED BSE AND TDDFT APPROACH

We now present an approach which combines the efficiency of the TDDFT method at high energies with the advantages of a local double-basis BSE approach near the edge. The approach makes it possible to treat the core-hole interaction and local-field effects over a wide spectral range. The full-response function is the main ingredient in the calculations of XAS beyond the independent-particle approximation, and it is given by the solution to the integral equation in Eq. (2),

$$\chi = \chi^0[1 - K\chi^0]^{-1}. \tag{5}$$

The term in brackets in Eq. (5),

$$\epsilon = [1 - K\chi^0], \tag{6}$$

is the dielectric matrix, and its inverse ϵ^{-1} is a key quantity of interest here. The four-point representation of $\chi^0(\mathbf{1},\mathbf{2},\mathbf{3},\mathbf{4},\omega)$ is formally given by

$${}^4\chi^0(\omega) = \sum_{ij}(f_i - f_j)\frac{\psi_i^*(\mathbf{1})\psi_i(\mathbf{3})\psi_j^*(\mathbf{2})\psi_j(\mathbf{4})}{\omega + E_i - E_j + i\Gamma}, \tag{7}$$

where $1 \equiv \mathbf{r}_1$, as in the notation of Onida *et al.*,[8] and the spin indexes are suppressed for simplicity. Here the one-particle states ψ_i are eigenstates of the quasiparticle Hamiltonian $h = p^2/2m + V_{coul} + \Sigma(E)$, where $\Sigma(E)$ is the self-energy and f_i are Fermi occupation numbers. In the examples of this paper $\Sigma(E)$ is calculated using the local GW plasmon-pole model of Hedin and Lundqvist. This self-energy and other quantities needed in the calculations such as the scattering potentials and phase shifts are obtained using the real-space multiple-scattering approach, which has been extensively tested for deep-core XAS.[9,15]

Next we separate the interaction kernel into local and nonlocal parts labeled K^L and K^N, respectively, by adding and subtracting a local exchange-correlation kernel, i.e.,

$$K^L(\mathbf{r},\mathbf{r}',\omega) = v(\mathbf{r},\mathbf{r}') + f_{xc}(r,r',\omega), \tag{8}$$

$$K^N(\mathbf{r},\mathbf{r}',\omega) = W(\mathbf{r}',\mathbf{r},\omega') - f_{xc}(\mathbf{r},\mathbf{r}',\omega). \tag{9}$$

Their description as *local* or *nonlocal* kernels is based on their behavior in the exchange integrals in response-function calculations, as discussed below. Also, K^L can be recognized as the TDDFT kernel, while K^N contains the nonlocal, screened, core-hole interaction. In general the exchange-correlation kernel is nonlocal and frequency dependent, but in practice the adiabatic local-density approximation (ALDA) is often used,[8]

$$f_{xc}^{ALDA}(\mathbf{r},\mathbf{r}') = \delta(\mathbf{r}-\mathbf{r}')\frac{\delta V_{xc}[\rho(\mathbf{r})]}{\delta\rho}, \tag{10}$$

where $V_{xc}[\rho]$ is the local-density approximation for the ground-state exchange-correlation potential. In this work we use the ground-state exchange correlation of von Barth and Hedin.[16]

Our combined approach for the interacting problem then consists of two steps:

(I) First, we apply the TDDFT method with a local kernel K^L yielding the local-density approximation to the TDDFT response function χ^L,

$$\chi^L = \chi^0[1 - K^L\chi^0]^{-1}. \tag{11}$$

If f_{xc} is neglected in K^L, the result is the RPA response function $\chi^L = \chi^{RPA}$. Our calculations of the local fields from χ^L follow a strategy similar to that of ZS, which we term the local-field time-dependent density-function theory (LFTDDFT) approach. We find that the calculation of XAS with the TDDFT response in χ^L is often adequate well above an edge over a broad energy spectrum.

(II) Second, the full response, including an explicit treatment of the screened core hole, is given by

$$\chi = \chi^L[1 - K^N\chi^L]^{-1}. \tag{12}$$

This result for the total response χ is formally equivalent to the BSE, since Eq. (12) implicitly includes the full K, but this step becomes increasingly difficult to implement as the photoelectron energy is increased. Fortunately we only need carry out this second step for energies within several eV of the edge, where the nonlocality of the screened core-hole interaction is most important. Our approach for this step is based on our projection-operator method,[14] which treats the screening of the core-hole interaction at the atomic level and is very efficient numerically. Here we will refer to this approach as the projection-operator method Bethe-Saltpeter equation (PMBSE).

III. LOCAL-FIELD EFFECTS

In this section we discuss step (I) of our combined approach. As noted above the TDDFT approach greatly simplifies the calculations, since with local exchange, the response function can be contracted to a two-point form. In particular the cross section can then be expressed in terms of the Fermi "golden rule," with a screened dipole interaction $\tilde{d}$.[5] That is, the dipole matrix elements within the TDDFT become renormalized,

$$\tilde{M}_{ij} = \int d\mathbf{r}d(\mathbf{r})[1 - K^L\chi^0]^{-1}\psi_i^*(\mathbf{r})\psi_j(\mathbf{r})$$
$$= \int d\mathbf{r}\tilde{d}(\mathbf{r})\psi_i^*(\mathbf{r})\psi_j(\mathbf{r}) \equiv \langle i|\tilde{d}|j\rangle. \tag{13}$$

The LFTDDFT approach was originally used to calculate the response for rare gas atoms using a Green's function method.[5] However this approach cannot be directly applied to extended systems. The reason is that the sum over a small number of occupied states in atoms, e.g., the 3*d* states of a transition metal element become an integral over the 3*d* valence band in solids. Hence the original ZS strategy needs to be modified. Our modifications for large molecules and solids are based on the real-space Green's function approach, as follows: (i) use solid-state scattering potentials instead of atomic potentials; (ii) include multiple scattering contributions in the propagator G to account for contributions from atoms in the environment of the absorbing atom; (iii) use a complex self-energy instead of ground-state LDA exchange-correlation potentials in the one-particle (quasiparticle) states; and (iv) use matrix inversion in real space, instead of an iterative solution for the local fields and the screened dipole coupling to the x-ray field $\tilde{d}$.

Since the response function in the core region, which dominates the screening in deep-core excitations, can be assumed to have rotational symmetry, it can be expanded locally in spherical harmonics,[17]

$$\chi(\mathbf{r},\mathbf{r}',\omega) = \sum_L Y_L(\hat{\mathbf{r}})\chi_l(r,r',\omega)Y_L^*(\hat{\mathbf{r}}'). \tag{14}$$

Thus the radial part of the screened dipole field $\tilde{d} = \tilde{d}(r)Y_{10}(\hat{\mathbf{r}})$ is determined by the $l=1$ component,

$$\tilde{d}(r) = \int dr'[1 - K^L\chi^0]^{-1}_{l=1}(r,r')d(r'). \tag{15}$$

Here $[1-K^L\chi^0]^{-1}_{l=1}(r,r') \equiv \epsilon^{-1}_{l=1}(r,r')$ defines the p-wave component of the dielectric matrix and $d(r)=r$ is the radial part of the dipole operator. In our applications for deep-core XAS we carry out matrix inversion explicitly in real space on the logarithmic, radial atomic grid of Desclaux[18] with a typical matrix size of 251×251, using only the absorbing-atom contribution to the response. Note that within the TDDFT with local kernels, the form of $\chi^0(\omega)$ is reduced to a function of only two space points, i.e., $\chi^0(\mathbf{r},\mathbf{r}',\omega)=^4\chi^0(\mathbf{r},\mathbf{r}',\mathbf{r}',\mathbf{r},\omega)$. This contraction is only possible when K is local. As in ZS, a Green's function representation of χ^0 is used,

$$\chi^0(\mathbf{r},\mathbf{r}',\omega) = \sum_i f_i\psi_i^*(\mathbf{r})\psi_i(\mathbf{r}')G(\mathbf{r},\mathbf{r}',E_i+\omega)$$
$$+ \sum_i f_i\psi_i^*(\mathbf{r}')\psi_i(\mathbf{r})G(\mathbf{r}',\mathbf{r},E_i-\omega). \tag{16}$$

Here G are retarded one-particle Green's functions which are formally given by

$$G(\mathbf{r},\mathbf{r}',E) = \sum_j \frac{\psi_j(\mathbf{r})\psi_j^*(\mathbf{r}')}{E - E_j + i\Gamma}, \tag{17}$$

where the summation runs over *all* of the eigenstates j of the quasiparticle Hamiltonian, and Γ accounts for lifetime broadening. In the calculations reported here, $G(E)$ is calculated using our real-space multiple-scattering codes.[9] The inclusion of the second *nonresonant* term in Eq. (16) is essential to forbid contributions between occupied and occupied or unoccupied and unoccupied states. Ensuring this cancellation requires considerable numerical care, but we have verified that the condition is satisfied to high accuracy in our calculations.

Remarkably the XAS can be calculated equivalently, using either the full-response function χ or in terms of local fields, as shown by ZS.[5] The latter approach is preferable here, since it requires only a modification of the transition matrix elements and leaves the fine-structure matrix $\chi_{L,L'}(E)$ unchanged. This is shown by Eq. (18) below with $\chi_{L,L'}$ defined in Eq. (19). Thus this approach can be readily applied to other spectroscopies, e.g., x-ray photoelectron spectros-

copy, where by examining the energy loss of the outgoing electron, one can see which core hole is left behind. It appears to be difficult to extract such partial quantities from the full-response function χ, where these contributions are mixed with the interactions K. However, this separation can be done straightforwardly in terms of the renormalized matrix elements $\tilde{M}_{iL}$.

Within the real-space multiple-scattering theory used here, the LFTDDFT approach yields an expression similar to the Fermi "golden rule" for the XAS cross section,[14]

$$\sigma(\omega) = \frac{4\pi\omega}{c} \sum_{i,LL'} f_i \tilde{M}_{iL}(\omega) \hat{\rho}_{L,L'}(E) \tilde{M}_{iL'}(\omega), \qquad (18)$$

where $E=\omega+E_i-E_F$. Here $\tilde{M}_{iL}(\omega)=\langle R_L|\tilde{d}|i\rangle$ are the screened dipole matrix elements from Eq. (13) in a relativistic angular-momentum basis $L=(\kappa,m)$, and $\rho(\mathbf{r},\mathbf{r}',E)=-(1/\pi)\mathrm{Im}\, G(\mathbf{r},\mathbf{r}',E)$ is the unoccupied one-electron density matrix, which in the real-space multiple-scattering formalism is given by

$$\rho(\mathbf{r},\mathbf{r}',E) \equiv \sum_i f_i \psi_i(\mathbf{r}) \psi_i^*(\mathbf{r}') \delta(E-E_i)$$

$$= \sum_{L,L'} R_L(\mathbf{r}) R_{L'}(\mathbf{r}') \rho_{L,L'}(E),$$

$$\rho_{L,L'}(E) = [\delta_{L,L'} + \chi_{L,L'}(E)]\theta(E-E_F). \qquad (19)$$

Here $R_L(\mathbf{r})$ are normalized scattering states calculated with only the absorbing-atom potential, and $\chi_{L,L'}(E)$ is the fine-structure matrix in XAS due to scattering from the environment.[9] Note that by replacing $\tilde{d}$ with the bare external x-ray field $d=\hat{\epsilon}\cdot\mathbf{r}$, the screened dipole-matrix elements $\tilde{M}_{iL}$ become bare dipole-matrix elements $M_{iL}=\langle R_L|d|i\rangle$ in Eq. (18), and one recovers the independent electron formula given by Fermi golden rule. Core-hole contributions can be included approximately in this expression in terms of the FSR. However, the use of fully screened core-hole potentials is not always satisfactory, as discussed in Sec. V below.

To illustrate the magnitude of the local fields, the ratio $\mathrm{Re}\,\tilde{d}(r)/d(r)$ of the local field to the bare x-ray electric field is shown in Fig. 2 for tungsten. The imaginary part of $\tilde{d}(r)$ (not shown) is also included in our calculations, but is significantly smaller. Clearly the screening effect is negligible in space beyond the extent of the initial $3d$ core orbital (solid curve in Fig. 2), and it slowly reduces in magnitude with increasing energy showing that our local approximation is satisfactory.

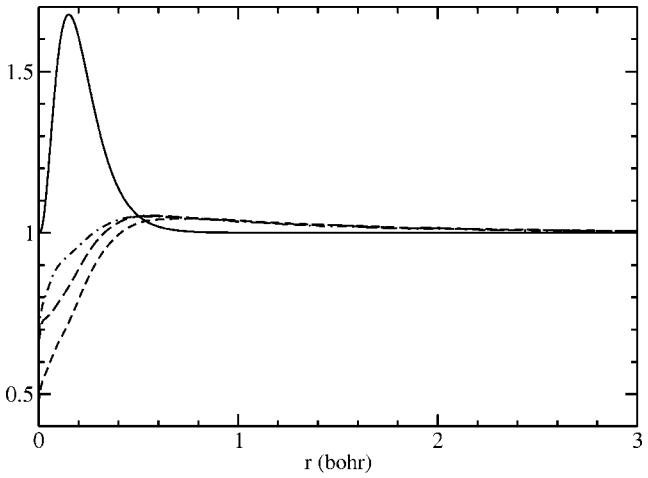

FIG. 2. Local-field effect: the real part of the ratio $\tilde{d}/d$ of the local screened x-ray field to the bare x-ray electric field is shown for photon energies above the tungsten M_5 edge at 1850 eV by 20 eV (dashes), 200 eV (long dashes), and 400 eV (dot-dashes). Note that the local fields are essentially restricted to the range of the initial-core orbital $[r\phi_{3d}(r)]$ (solid line), which for clarity is shifted vertically by unity.

IV. NONLOCAL CORE-HOLE INTERACTION

In this section we discuss part (II) of our combined procedure, in which the nonlocal interactions in K^N are treated. This step requires an explicit calculation of the screened core-hole interaction given by Eq. (11) for χ in terms of χ^L. Thus we must first evaluate the local-response function χ^L using

$$\chi^L = \chi^0 + \chi^0 K^L \chi^L = \chi^0 + \chi^0 W^L \chi^0, \qquad (20)$$

where W^L defines the local screened-exchange interaction,

$$W^L = [1 - K^L\chi^0]^{-1} K^L = \epsilon_L^{-1} K^L. \qquad (21)$$

Second we must calculate the full response χ from Eq. (12). The above relations are applicable both for two-point and four-point forms of χ. Here we need a four-point form, which we calculate as in a previous work,[14]

$${}^4\chi^0(\omega) = \sum_i f_i \psi_i^*(\mathbf{1}) \psi_i(\mathbf{3}) \int_{E_F}^{\infty} \frac{dE}{\pi} \rho(\mathbf{2},\mathbf{4},E)$$

$$\times \left[\frac{1}{\omega - E + E_i + i\Gamma} + \frac{1}{\omega + E - E_i + i\Gamma} \right]. \qquad (22)$$

Next, we make use of the local atomic-projection operator $\hat{P}$ to approximate this local screened-dipole interaction,[14] i.e., $\hat{P}=\Sigma_n|\psi_n\rangle\langle\psi_n|$. This operator projects a given function onto a local basis set of atomiclike orbitals at the central absorbing atom. Then the density matrix can be approximated by its local contribution, $\rho\approx\rho^{loc}=\hat{P}\rho\hat{P}$. This approximation can be systematically improved by including a more complete set of states n. Consequently, the response function ${}^4\chi^0$ with our projection method becomes

$${}^4\chi^0(\omega) = \sum_{inn'} f_i \psi_i^*(\mathbf{1}) \psi_n^*(\mathbf{2}) \chi^0_{in,in'}(\omega) \psi_i(\mathbf{3}) \psi_{n'}(\mathbf{4}),$$

$$\chi^0_{in,in'}(\omega) = \frac{-2k}{\pi} \sum_{L,L'} \int_{E_F}^{\infty} dE \frac{\langle\psi_n|R_L\rangle \rho_{L,L'} \langle R_{L'}|\psi_{n'}\rangle}{\omega - E + E_i + i\Gamma}, \qquad (23)$$

where $k=\sqrt{2(\omega+E_i)}$. Note that the localized part of χ^0 does not require a Kramers-Kronig transform at each space point, since the localized part of the photoelectron wave function

can be separated into energy- and position-dependent parts. Moreover, the overlap matrices decay quickly with energy, so the Kramers-Kronig transform converges well. This significantly simplifies the calculations and allows us to use a fast-matrix formulation similar to that of Schwitalla and Ebert.[6] A similar expansion also can be applied to the local (or RPA) response

$$^4\chi^L(\omega) = \sum_{in,i'n'} f_i f_{i'} \psi_i^*(\mathbf{1})\psi_n^*(\mathbf{3})\chi^L_{in,i'n'}(\omega) \times \psi_{i'}(\mathbf{2})\psi_{n'}(\mathbf{4}),$$

$$\chi^L_{in,i'n'} = \chi^0_{in,i'n'} + \chi^0_{in,i_1n_1} W^L_{i_1n_1,i_2n_2} \chi^0_{i_2n_2,i'n'}, \tag{24}$$

where the interaction $W^L(\mathbf{r},\mathbf{r}',\omega)$ is obtained from Eq. (9), and its matrix elements $W^L_{i_1n_1,i_2n_2}$ are straightforward to calculate, as discussed below.

The equations for the renormalized transition-matrix elements are similar to those with the projection-method approach introduced previously,[14]

$$\tilde{M}_{in} = M_{in} + K^N_{in,i'n'} \tilde{\chi}^L_{i'n',i''n''}(\omega) \tilde{M}_{i''n''}, \tag{25}$$

$$K^N_{in,i'n'}(\omega) = \int d\mathbf{r} d\mathbf{r}' \psi_i(\mathbf{r}) \psi_n^*(\mathbf{r}) \times K^N(\mathbf{r},\mathbf{r}',\omega) \psi_{n'}(\mathbf{r}') \psi_{i'}^*(\mathbf{r}'). \tag{26}$$

Here $\tilde{M}_{in} = \langle \psi_n | \tilde{d} | i \rangle$; however, these matrices can be calculated directly by matrix inversion,

$$\tilde{M} = M + K^N \chi^L \tilde{M} = [1 - K^N \chi^L]^{-1} M. \tag{27}$$

Clearly this approximation mixes the various angular-momentum channels and is responsible, for example, for the deviation of the L_3/L_2 intensity ratio from the statistical value of 2 in the one-electron approximation. The screened transition-matrix $\tilde{M}_{iL}$ elements needed to calculate the cross section are also given by Eqs. (25) and (26), with the replacement $\psi_n \rightarrow R_L(E)$ for each E.

As a consequence of the locality of the exchange-correlation kernel $f_{xc}[\rho(\mathbf{r})]$, the direct and exchange-correlation contributions to $K_{iL,i'n'}(\omega)$ satisfy the same selection rules and can all be calculated using the standard relativistic formulas for the matrix elements of the electrostatic interaction.[19]

V. SCREENED CORE-HOLE INTERACTION

Finally we discuss our treatment of the screened core-hole interaction W, which is needed in the direct kernel K^N above. An accurate treatment of the screening of the core-hole interaction potential is usually essential in quantitative calculations of XAS. However, the extent of such screening is material dependent, and various *ad hoc* prescriptions, such as the FSR or the $Z+1$ approximation, which are screened to all orders, can give too much screening. In contrast, the approach adopted here provides a systematic approach for calculating the screening effects within the RPA. In general the screened matrix elements of K^N can be frequency dependent, e.g.,

$$K^N_{in,i'n'} = \int d\mathbf{r} d\mathbf{r}' \psi_i(\mathbf{r}) \psi_{i'}^*(\mathbf{r}) \mathrm{W}(\mathbf{r},\mathbf{r}',\omega_{ii'}) \times \psi_n^*(\mathbf{r}') \psi_{n'}(\mathbf{r}'), \tag{28}$$

where $\omega_{ii'} = |E_i - E_{i'}|$. For deep core XAS the core hole is highly localized near the nuclei [cf. Fig. 2], and therefore W is predominantly spherically symmetric. Thus it can couple substantially only the states with the same total momentum for the core-hole state $j(i) = j(i')$, and coupling for $i \neq i'$ can be neglected. Then the screened core-hole interaction simplifies, and a static approximation can be used,

$$K^N_{in,i'n'} \approx \delta_{i,i'} \int dr' \tilde{V}_i(\mathbf{r}') \psi_n^*(\mathbf{r}') \psi_{n'}(\mathbf{r}'), \tag{29}$$

$$\tilde{V}_i(\mathbf{r}) = \int d\mathbf{r}' \psi_i(\mathbf{r}') \psi_i^*(\mathbf{r}') W(\mathbf{r}',\mathbf{r}), \tag{30}$$

where $W(\mathbf{r},\mathbf{r}') = W(\mathbf{r},\mathbf{r}',\omega=0)$, and $\tilde{V}_i(r)$ represents the core-hole potential for core-level i. BSE calculations usually use a statically screened interaction W, as calculated with a linear response using the RPA,[8]

$$W = v + v\chi^0 W = [1 - v\chi^0]^{-1} v. \tag{31}$$

Calculations of the screened core-hole interaction simplify in the static limit. Also due to the spherical symmetry of deep core-hole states, only the s-wave ($l=0$) component of the response function is needed. Again, using the formalism of Stott and Zaremba,[17] the s-wave component of the response is calculated using

$$\chi^0_{l=0}(r,r') = -\frac{1}{2\pi} \mathrm{Im} \int^{E_F} \frac{d\omega}{\pi} \sum_{l=0}^{\infty} (l+1) G_l^2(r,r',\omega). \tag{32}$$

Then Eq. (31) for W is evaluated by inverting $[1 - v\chi^0]^{-1}_{l=0}(r,r')$ in real space on a radial grid.

It is interesting to compare the RPA-screened core potentials $\tilde{V}_i$ with the fully screened potentials from the FSR. These potentials can be viewed as a difference in total self-consistent field (SCF) potentials (i.e., ΔSCF method) with and without the core-hole,

$$\tilde{V}_i^{FSR}(r) = V_i(r) - V^0(r), \tag{33}$$

where $V_i'(r)$ is the total SCF potential with a core hole in level i, and $V^0(r)$ is the ground-state potential.

As an illustration, Fig. 3 shows our calculations of the screened core-hole potential for tungsten. Here the solid curve is the bare, unscreened potential, which behaves as $1/r$ at large distances. The dotted curve shows the screened core-hole potential calculated by linear response (i.e., the RPA with $K^L = v$), and the dashes show the FSR potential. Both core-hole potentials are comparable and the sensitivity of the XAS to the core-hole potential is shown in Fig. 4.

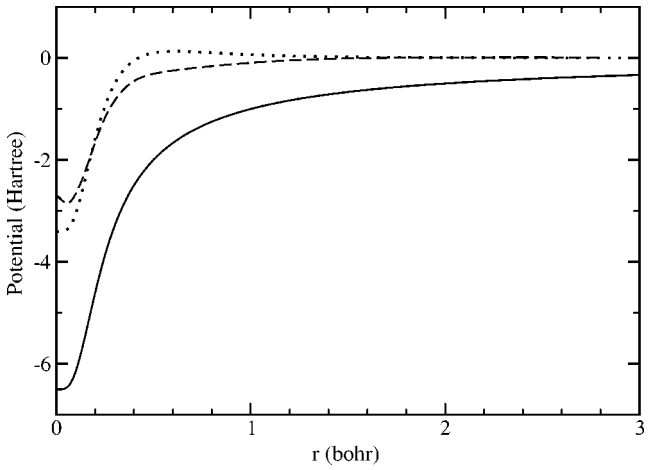

FIG. 3. Core-hole potential. The bare core-hole potential for the M_5 level of tungsten (solid) compared to the RPA screened potential (dots), and the fully-screened FSR potential (dashes).

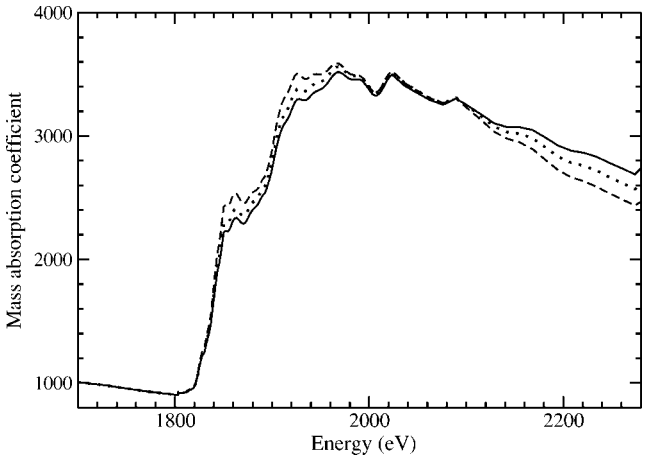

FIG. 4. Mass-absorption coefficient (cm^2/g) near the M_5 edge of tungsten. LFTDDFT calculations (solid) compared to PMBSE for two different core-hole potentials: RPA-screened potential (dots) and FSR potential (dashes).

VI. RESULTS AND DISCUSSION

We have chosen a few examples to illustrate our approach in different screening limits. In particular the case of *M*-shell XAS in *W* illustrates one limit, where the core-hole interaction is weak (being strongly screened) and local-field effects dominate. The case of *K*-edge XAS in MgO represents the other limit, where the core-hole interaction dominates. The case of the L_3-edge XAS of Ni metal is intermediate, where both effects are strong and tend to cancel.

Figure 1 shows the effect of including local-field effects in the calculations for *W*. Note that calculations with only the local TDDFT method (solid line) do not treat the nonlocal core-hole potential, while our PMBSE approach (dotted line) loses accuracy at energies high above the edge. Also note that the LFTDDFT and the PMBSE both reasonably account for the corrections to the independent-electron approximation within the first 200 eV from the edge. The agreement between these different approaches serves as a check on the various numerical approximations in the calculations. Finally note that our combined approach for the absolute cross section, which has no adjustable parameters, agrees with the experiment to within experimental uncertainty.

Figure 4 shows the effect of including the core-hole interaction in calculations for tungsten. Here the solid line is the same as that in Fig. 1, and it corresponds to our LFTDDFT approach with the neglect of the core-hole interaction. The dotted curve shows our full TDDFT-BSE calculation with the RPA-screened potential, while the dashed curve shows the full calculation with the FSR core hole. For this case it is clear that the local-field effect on the spectra is much stronger than that of the core-hole interaction. A smaller effect from the RPA-screened potential might have been expected, since it is positive at higher distances, as discussed above.

Next Fig. 5 shows calculations for the Ni near the L_3 edge. Here both the core-hole and local-field effects are important, despite the fact that the single-electron calculations (dots) gives a good agreement with the experiment. The reason is that the two effects are of opposite sign and tend to cancel. Thus RPA calculations (thin solid) show a significant reduction of the L_3 white line. However, the addition of the FSR core-hole potential restores the intensity of the L_3 white line. For this case the results appear to be very sensitive to the screening of the core-hole potential. Thus we find a best agreement with the experiment if we use a mixed potential, where about 80% of the core-hole interaction is taken from the RPA-screened potential and 20% from bare core-hole potential.

Finally Fig. 6 shows our results for the *K* edge of MgO. This is the opposite limiting case, where the core-hole-interaction effect is stronger than that from the local fields. This is likely due to the generally weaker screening in insulators than in metals. The standard real-space multiple-scattering calculations based on the FEFF8 code,[10] which includes a fully screened core-hole from the FSR, also give good results (Fig. 6, dashes), since the local-field effect is small for MgO. The results obtained with the combined ap-

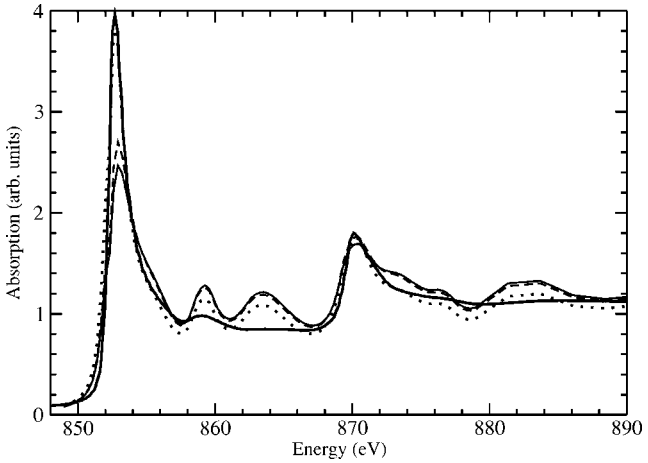

FIG. 5. Ni L_3-edge and L_2-edge absorption. The LFTDDFT calculations (solid) as compared to independent particle approximation (dots) and experiment (thick solid). The dashes show calculations with a fully-screened FSR core-hole potential.

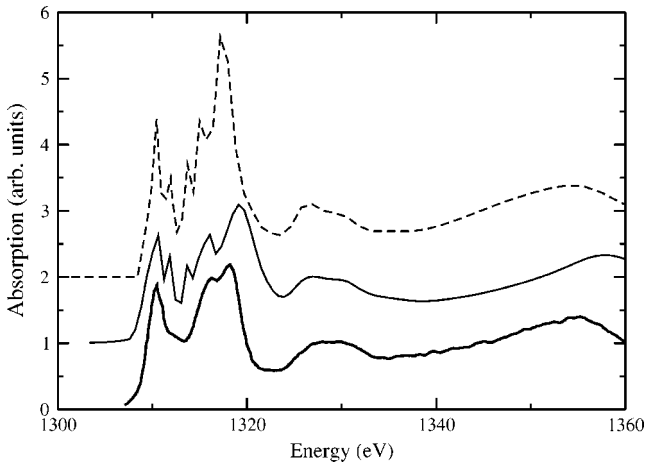

FIG. 6. X-ray absorption for the Mg *K* shell of MgO. Note that our combined approach (solid) significantly improves the intensity of the two leading peaks compared to the experiment (Ref. 20) (thick solid) or final-state-rule calculations (dashes).

proach of this paper (Fig. 6, thin solid line) compare well with the experiment.[20] In particular, we find that the ratio of the two largest peaks is very sensitive to the core-hole potential $W(r)$. Therefore the improvement of the intensity of the second peak compared with that in the experiment is mainly due to our improved calculation of W with the Stott-Zaremba method. For these MgO calculations we treat the local-field effects via the LFTDDFT method (I) and include the core-hole potential using the PMBSE (II). For both I and II, we set $f_{xc}=0$, since this cancels in the sum K^L+K^N in Eqs. (8) and (9). Within II, we only use a single $3p$-orbital for the projection-method basis set.

VII. SUMMARY AND CONCLUSIONS

We have developed a combined TDDFT-BSE approach for calculations of x-ray spectra beyond the independent-particle approximation that includes the effects of local fields from the screening of the x-ray field and a screened core-hole interaction. In this combined approach, the response function from the LFTDDFT approach is used in the subsequent calculation of the full BSE response function to account for the nonlocal, screened core-hole interaction. A key step in the combined approach is the construction of the full four-point response function, using results obtained from the two-point response function, as calculated within TDDFT or the RPA. Our treatment also includes inelastic losses and self-energy shifts based on the quasiparticle approximation, as implemented in our real-space multiple-scattering codes.[9]

Our combined approach has several practical advantages. First, the LFTDDFT approach is very efficient, compared to the BSE, and it is applicable over a wide spectral range above the edge. Second, the precise form of the exchange-correlation kernel $f_{xc}(\rho)$ appears not to be crucial away from the edge, obviating the need for special or nonlocal kernels. Third, the approach yields the full BSE response near the edge, where nonlocal effects are most important. Moreover, the method elucidates the nature of the screening, both of the x-ray field and of the core hole in a system-dependent manner, and thus explains why one or the other of these effects can dominate in a calculation.

Our combined approach has been implemented using first an extension of the LFTDDFT approach of ZS, which provides a practical generalization of their approach for molecular or condensed systems. The second part of our procedure is an implementation of the BSE, which is applicable in the near-edge region. For this part we use a local-projection method,[14] which has been extended here to treat the nonlocal screened core-hole interaction. Since the two-particle interaction effects K^X and K^D are of opposite signs and tend to cancel, the results can be sensitive to the details of the core-hole-potential construction and screening. Our calculations make use of the adiabatic formalism of Stott and Zaremba[17] to evaluate the screened core-hole interaction.

We find that our combined approach works well, both for cases in which the local-field effect dominates, e.g., W, and where the core-hole interaction dominates, e.g., MgO. In particular the calculations with no adjustable parameters agree with the absolute measurements to within experimental uncertainty. Thus this approach provides an efficient method for general calculations of x-ray spectra and other optical constants, over a broad spectrum from UV to x-ray energies.[21] Moreover, the ideas behind our combined approach are not restricted to the present application, and they may be used to extend the utility of existing TDDFT and BSE codes.

ACKNOWLEDGMENTS

We thank A. Soininen and E. Shirley for suggestions and for a critical reading of the manuscript. We also thank Z. Levine for making available the experimental W and Ta data, and G. Bertsch, J. Chelikowsky, A. Nesvizhskii, S. Pantelides, and L. Reining for useful comments. This work was supported by DOE Grant Nos. DE-FG03-97ER45623 and DE-FG03-98ER45718 and was facilitated by the DOE Computational Materials Science Network.

[1] G. Strinati, Phys. Rev. B **29**, 5718 (1984).
[2] J. A. Soininen and E. L. Shirley, Phys. Rev. B **64**, 165112 (2001).
[3] M. Rohlfing and S. G. Louie, Phys. Rev. B **62**, 4927 (2000).
[4] L. Reining, V. Olevano, A. Rubio, and G. Onida, Phys. Rev. Lett. **88**, 066404 (2002).
[5] A. Zangwill and P. Soven, Phys. Rev. A **21**, 1561 (1980).
[6] J. Schwitalla and H. Ebert, Phys. Rev. Lett. **80**, 4586 (1998).
[7] I. Vasiliev, S. Ögut, and J. R. Chelikowsky, Phys. Rev. Lett. **82**, 1919 (1999).
[8] G. Onida, L. Reining, and A. Rubio, Rev. Mod. Phys. **74**, 601

(2002).
[9] A. L. Ankudinov, B. Ravel, J. J. Rehr, and S. D. Conradson, Phys. Rev. B **58**, 7565 (1998).
[10] J. J. Rehr, J. A. Soininen, and E. L. Shirley, Phys. Scr. (unpublished).
[11] See, e.g., R. Buczko, G. Duscher, S. J. Pennycook, and S. T. Pantelides, Phys. Rev. Lett. **85**, 2168 (2000).
[12] J. C. Slater, *Quantum Theory of Molecules and Solids* (McGraw-Hill, New York, 1974).
[13] Z. H. Levine, S. Grantham, C. Tarrio, D. J. Paterson, I. McNulty, T. M. Levin, A. L. Ankudinov, and J. J. Rehr, J. Res. Natl. Inst. Stand. Technol. **108**, 1 (2003).
[14] A. I. Nesvizhskii, A. L. Ankudinov, and J. J. Rehr, Phys. Rev. B **63**, 094412 (2001).
[15] J. J. Rehr and R. C. Albers, Rev. Mod. Phys. **72**, 621 (2000).
[16] U. von Barth and L. Hedin, J. Phys. C **5**, 1629 (1972).
[17] M. J. Stott and E. Zaremba, Phys. Rev. A **21**, 12 (1980).
[18] J. P. Desclaux, Comput. Phys. Commun. **9**, 31 (1975).
[19] I. P. Grant, Adv. Phys. **19**, 747 (1970).
[20] T. Lindner, H. Sauer, W. Engel, and K. Kambe, Phys. Rev. B **33**, 22 (1986).
[21] G. Rivas, J. J. Rehr, A. L. Ankudinov, and M. Prange (unpublished).